ROMA TRE UNIVERSITY

Department of Mathematics and Physics

Bachelor degree course in Physics

Bachelor Degree Thesis

The Modeling of Scintillation Detectors with Geant4

Supervisor:
Prof. Domizia Orestano

Candidate:
Pietro Meloni

Academic Year 2017-2018

Statement of Translation:

I, Pietro Meloni, declare that this document is a true and accurate translation of the Italian version titled "Modellizzazione con Geant4 di rivelatori a scintillazione" and filed at the office of Roma Tre University.

Pietro Meloni
Signature

19/12/2018
Date

Contents

Chapter 1

Introduction

In particle physics, the use of simulations has gradually gained importance, and nowadays, its role is fundamental for designing new detectors. Indeed, a simulation is a valuable tool for establishing which materials and geometric properties are more appropriate for a detector. Moreover, currently, simulations are sufficiently precise and powerful for comparing real data with theoretical models and searching for new Physics phemomena, beyond the *Standard Model*.

This thesis aims to create a model of a scintillation detector and, by using Geant4 [1], simulate its response to given radiation. The choice of this particular detector has been suggested by the possibility to further a didactic experiment carried out within the *Nuclear and Subnuclear Physics Laboratory* (NSPL). The experiment consisted in characterizing a scintillation detector and measuring the flux of cosmic rays at sea level. The continuity between this work and the laboratory activities has made it possible to compare simulated results with experimental data.

Before we continue describing the simulation, we shall introduce both scintillation detectors and Geant4.

1.1 Scintillation detectors

Scintillation detectors represent a class of detectors that emit light when exposed to ionizing radiation. These detectors are made up of a sensitive part – the *scintillator* – and one or more *photomultipliers* capable of converting light signals into measurable electric signals.

Scintillators

Scintillator luminescence is due to the emission of photons which, in turn, is due to the de-excitation of atomic (or molecular) electrons, previously excited by the passage of a charged particle through the material. The emission spectrum covers the binding energy of atoms and molecules, namely, the ultraviolet and the visible band. The de-excitation is exponential time-dependent with characteristic time τ. The emission process is called *fluorescence* when $\tau_f \sim 10$ ns, while it is known as *phosphorescence* when the excited state is metastable, and the emission occurs in a $\tau_s \sim 1$ ms [2].

The properties of a scintillator determine its use and the possible measurements to perform with it. For instance, a material with high efficiency (i.e., photons emitted per energy loss unit) is particularly useful for detecting particles that lose little energy.

A scintillator which is transparent to its own emitted light is more appropriate for large scintillation detectors, where light has to travel long distances before reaching the photomultipliers. In more sophisticated detectors, scintillators can be made more transparent by using *wavelength shifters*, i.e., fluorescent materials that absorb light with a specific frequency and re-emit it at a lower one [3].

A scintillator with a characteristic time τ of few nanoseconds is, instead, ideal for time measurements, hence, it can be used as a *trigger* in more complicated detectors.

Ultimately, an important feature that is common to any good scintillator is the linearity, namely, the proportionality between energy loss and light emitted.

Generally, to prevent any leak of light from the material as well as to reduce the noise due to environmental light, scintillators are first wrapped in a reflective material (e.g., aluminum), and then covered with an opaque material, usually black.

Photomultiplier tubes

A photomultiplier tube (PMT) is an electronic detector sensitive to ultraviolet, visible and near infra-red bands. Its functioning is based on two processes: the photoelectric effect and the secondary emission (i.e., the electro-multiplication). A PMT, such as the one in Figure 1.1, consists of an input window, called *photocathode*, a multiplying section, and an anode. On the photocathode, which is made of a photosensitive material, photons are converted into electrons via the photoelectric effect. Once produced, electrons are accelerated by an electric field through the multiplying section which is made up of a certain number of electrodes, called *dynodes*. On each dynode, secondary electrons are generated via electro-multiplication. On the anode, all the secondary electrons are collected, and the corresponding current can be analyzed.

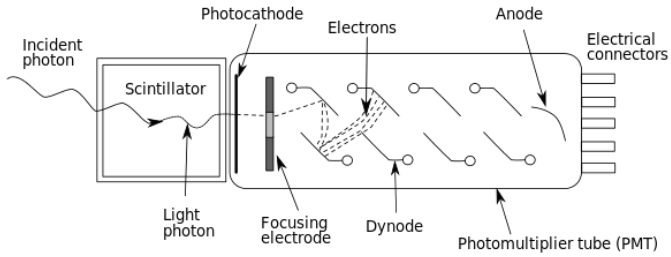

Figure 1.1. Scheme of a PMT coupled to a scintillator.

As a detector, a PMT is affected by different types of noise. One cause of noise is the dark current due to the thermal noise of dynodes. This effect can be reduced by decreasing the working temperature. Another cause of noise is, instead, the after-pulse, namely, residual gases or radioactive materials in the phototube that, when ionized by electrons, generate currents with delays of 30-60 ns [2].

While designing a scintillation detector, the coupling between PMTs and the scintillator is an aspect of utmost importance. In fact, in order to increase the number of photons that undergo the photoelectric effect, it is necessary to maximize the overlapping between the emission spectrum of the scintillator and the spectral response of the photocathode. We shall discuss this aspect more in-depth later.

1.2 Monte Carlo methods and Geant4

Monte Carlo methods are a wide class of computational techniques consisting in sampling random numbers to solve numeric problems. Any Monte Carlo method involves algorithms that generate a set of random numbers with a certain probability distribution. Monte Carlo methods are used in several fields, including simulations of particle physics experiments. Among the available software for simulating the passage of radiation through matter we have choosen Geant4 (*GEometry ANd Tracking*). Geant4 is a toolkit that makes use of an object-oriented programming language (C++); hence, any tool is described by a specific *class*. A diagram of the main classes of Geant4 is shown in Figure 1.2. Each box represents a class, and the lines show the relations among classes.

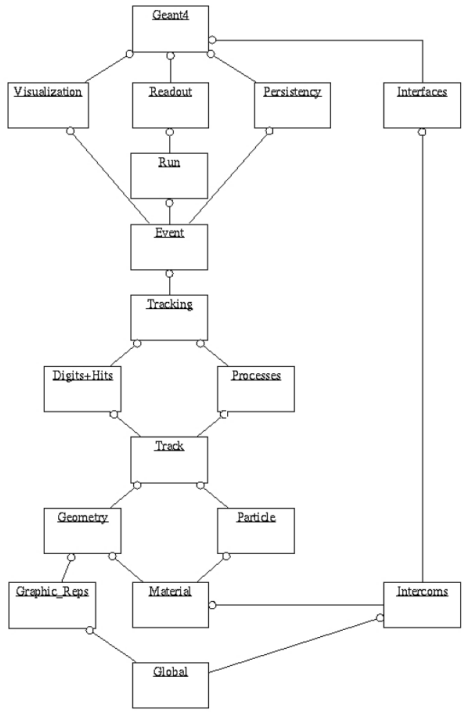

Figure 1.2. Geant4 class diagram [1].

Now, we shall discuss some classes and tools represented in the scheme – in particular those used in the simulation.

In Geant4, the following objects must be defined by the user prior to any simulation: *primaries*, detector, and physics models. The primaries are the initial particles that, by interacting with the detector, generate the *secondaries*, namely the secondary particles. To set the primaries, it is necessary to define the primary generator. The implementation of a detector involves setting its geometry and materials. A proper choice of the physics models allows the user to select the phenomena of interest, but also to prevent the simulation from being slowed down.

In a simulation – as well as in a real experiment – an *event* is everything that occurs starting from the primaries generation until the absorption of all of the secondaries. In Geant4, all the information on primaries, secondaries and their trajectories are stored in event-like objects.

A collection of events sharing the same physical conditions and the same detector is called *run*. Both events and runs are managed by specific classes, and the user can access all their information 'invoking' specific methods.

In a simulation, a track is a snapshot of a particle at a given time. A track-type object holds all the information on the dynamic properties at a certain time. A track is updated via several *steps*. Each step is delimitated by two points (i.e. *pre* and *post step point*) which is particularly useful for simulating boundary processes (e.g., reflection and refraction). The step length depends on the material and on the crossing sections of possible processes in that material [1].

Ultimately, in order to manage and analyze the results of the simulation, the user can define new specific classes. For this purpose, in Geant4, it is possible to use different libraries. In this case, we have used ROOT.

Further information about Geant4 and its use in this work can be found in Appendix A.

Chapter 2

Project

As we have mentioned, the aim of this work is to create a model of a detector similar to those used in the NSPL course. In particular, the detector will be a plate of scintillation material with two PMTs placed on the short sides. Materials, dimensions and technical details will be discussed in the next chapter. In this section, instead, the scheme of the simulation will be explained.

The simulation was designed with a block structure, to allow the user to test different parts of the code, and to produce results with different levels of approximations. In particular, it has been useful to think of any process or detector part as a method, i.e. a function, that takes input and returns output.

2.1 Project description

As shown in the diagram in Figure 2.1, each event begins with the primary generator that sets the initial particles, in the specific case muons. The generator samples five random numbers from given probability distributions that we will discuss later. Such numbers describe the initial energy E of the primary, the coordinates x and y of the primary's point of impact on the scintillator, and inclination θ and ϕ with which the primary hits the detector.

The numbers so generated are used to calculate the distance $\Delta\ell$ traveled by the primary through the scintillator. As shown in the diagram, this computation can either be implemented on the basis of geometric reasoning or via Geant4 classes and methods. Similarly, two different ways can be followed to calculate the energy ΔE lost by the particle in the detector. One possible way involves the Bethe-Block formula, whereas the other one exploits – again – the specific Geant4 methods (which include the Bethe-Block formula as well).

Once the energy loss ΔE is known, it is possible to simulate the scintillation

process and count the number of photons generated. The parameter which defines the number of photons emitted per unit energy is the *light yield* (ε), or efficiency, of the material.

The propagation of photons will be simulated starting from their emission point up to one of the two photocathodes. For this purpose, reabsorption and reflections will be implemented. The parameters that define these two processes are the absorption length (λ) of the scintillator, and the reflectivity (r) of the material that covers it. The method corresponding to this part of the simulation will count the number of photons that reach the photocathodes, as well as their energy and the arrival time.

Once the number of photons collected at the photocathode is known, the photoelectric effect will be simulated, producing a certain amount of primary electrons. Thus, we will simulate the multiplication of electrons through the dynode section. This part can be implemented by either taking into account the overall gain, or by applying the single dynode gain for all the dynodes.

The final result will be an overall number of electrons and their arrival time at the photocathode. Hence, it will be possible to reproduce the current signal (or the tension signal) corresponding to the passage of a muon. In the end, by setting the proper threshold voltage, signals can be discriminated.

2.2 Simplifications and approximations

During the design phase, some approximations have been made. We have not considered the light guide that connects the PMT to the scintillator. In this simplification, a small part of photons absorbed in the guide has been neglected, as well as possible fluctuations of the time delay of photons at the photocathode. In a similar way, time delays of photons in PMTs have been neglected. Ultimately, a significant simplification is the total absence of noises, in both the PMTs and the scintillator.

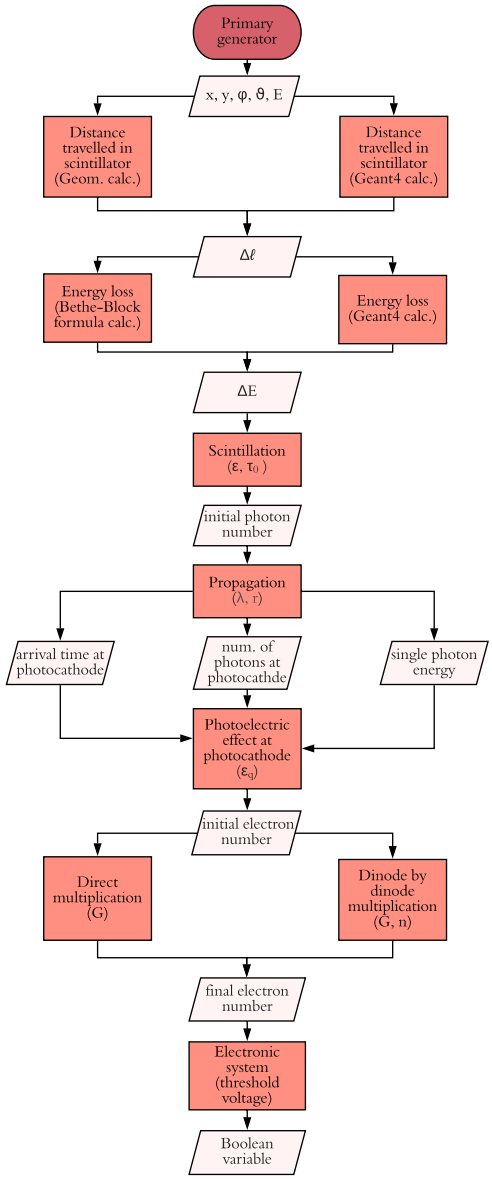

Figure 2.1. Diagram of the simulation: the upper oval represents the primary generator; the rectangular blocks are physical processes and detector parts; the parallelograms represent input and output of the other blocks.

Chapter 3

Simulation

In this chapter, we will describe the simulation and its results, by following the project just explained. We shall begin with outlining the geometry and materials of the detector, together with the physical processes allowable in the simulation.

3.1 Choice of the physical processes

In a simulation, it is not interesting – nor convenient – to reproduce all the possible physical processes. Hence, Geant4 makes it possible to select processes and particles to use in the simulation. In this specific work the following particles and processes have been made possible:

- neutrons, protons, electrons, positrons, neutrinos, photons, muons, pions;
- multiple scattering and ionizing processes, photoelectric effect, decays.

The fact that each process can be defined singularly is extremely useful because – as we will see later – it allows the user to test the simulation by turning on (or off) specific processes.

3.2 Geometry and materials

The detectors used in the NSPL course – which this simulation is inspired by – consisted of a plate (122 cm x 20 cm x 1 cm) of a plastic scintillator (UPS89) with two PMTs Photonis XP2262 placed on the two short sides. A detector similar to those in the laboratory has been implemented in Geant4 and it is represented in Figure 3.1. The light guides are shown in the figure, although the light passage through them will not be simulated. On the contrary, the PMTs are not depicted

in the image, though they have been implemented in the simulation. As a material for the scintillator, we have chosen polystyrene.

The Coordinate system has been chosen as in Figure 3.1: with the origin in the symmetrical center of the plate, with the z axis perpendicular to the plate, and x and y axes parallel respectively to the short and the long side.

Further properties of materials and surfaces of the detector will be introduced later. Moreover, we will change some features, such as the material, to test the accuracy of the results.

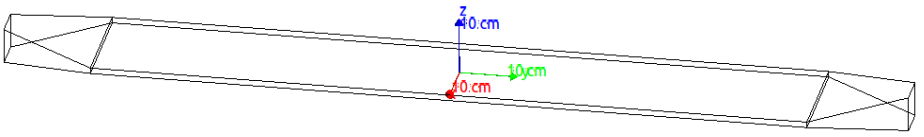

Figure 3.1. Schematic image of the detector. At the two extremities, the light guides are represented even though they are not included in the simulation.

3.3 Primary generation

As in the NSPL course, cosmic rays at sea level will be the primaries. Indeed, only muons (μ^+ e μ^-) will be taken into consideration as a principal component ($\sim$70%) of cosmic rays at such an altitude [4]. The number of μ^+ and μ^- has been made statistically equal by sampling values from a Bernoulli distribution with two possible, and equiprobable, values.

As already mentioned in the project, the generation of a primary consists of sampling five pseudo-random numbers: the coordinates x and y of the muons' point of impact on the scintillator; the polar angle ϕ and azimuthal angle θ that identify the inclination with which the muon hits the scintillator; the initial energy E of the muon. It is reasonable to assume there are no preferred values of x and y; thus, we will assume both these numbers to be uniformly distributed between their maxima (10 cm and 61 cm) and minima (-10 cm and -61 cm). Moreover, it is experimentally well known that the differential flux of muons at sea is independent of ϕ and proportional to $\cos^2\theta$, namely:

$$I(\theta,\phi) = \frac{dN}{dAdtd\Omega} = I(0)\cos^2(\theta) \tag{3.1}$$

Hence, ϕ is uniformly distributed between zero and 2π, whereas θ is distributed as $\cos^3(\theta)\sin(\theta)$ with θ between zero and π. The $\cos(\theta)\sin(\theta)$ factor comes from the fact that the differential flux is defined as the number of particles that go through a horizontal surface element arriving from a unit solid angle, per unit time.

For energy, at this stage, we fix a value of 3 GeV, compatible with the average energy of muons at sea level [4]. However, a value of 1 GeV will be also used later, to test the simulation.

To facilitate the following analysis, we have fixed the height z at which muons are generated so that they hit the scintillator as soon as they are created, namely z =0.5 cm.

Once the five distributions have been defined, and the initial height z has been established as above, the actual simulation can start. At this stage, it is not yet possible to perform any quantitative analysis. However, we can visualize the generation of primaries as in Figure 3.2.

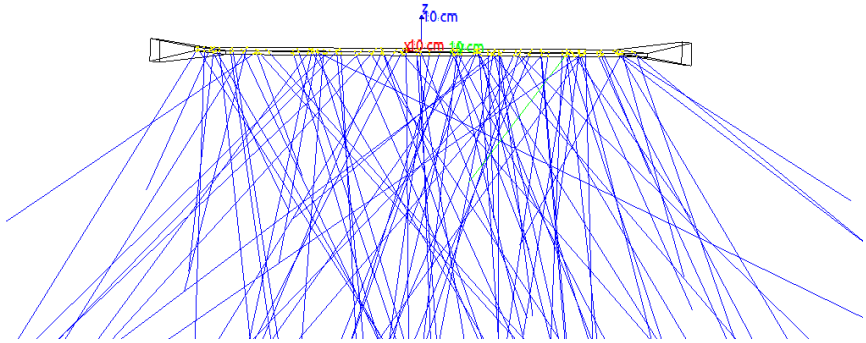

Figure 3.2. Visualization of a run of 100 muons hitting the detector. Muons are generated on the upper surface of the scintillator (z =0.5 cm), as set in the generator.

3.4 Distance traveled in the scintillator

Once the primary generator has been implemented, we can proceed with the computation of the distance $\Delta\ell$ traveled by muons in the scintillator. This operation, as already mentioned, can be performed either by using classes and methods of Geant4, or via simple geometric considerations.

Geometric computation

Consider a muon denoted by the values x_0, y_0, θ_0 and ϕ_0 sampled by the generator. It is possible to define the intersection point between the muon track and the lower

surface of the scintillator. Let x_1 and y_1 be the coordinates of such a point. If we assume the trajectory to be a perfectly straight line – that is, if multiple scattering is neglected – x_1 and y_1 are expressed by the following relations:

$$\begin{cases} x_1 = x_0 - d \tan\theta_0 \cdot \cos\phi_0 \\ y_1 = y_0 - d \tan\theta_0 \cdot \sin\phi_0 \end{cases} \tag{3.2}$$

where $d = 1$ cm is the scintillator width. Thus, the distance traveled through the scintillator reads:

$$\Delta\ell = \sqrt{(x_0 - x_1)^2 + (y_0 - y_1)^2 + d^2} \tag{3.3}$$

This geometric reasoning works as long as the muon actually reaches the lower surface of the scintillator and does not exit sideways. It has been estimated that, when d = 1 cm, around 97% of the muons generated fulfills this condition. For the remaining 3%, it is reasonable to assume $\Delta\ell$ to be uniformly distributed between zero and 1 cm.

Geant4 computation

It is also possible to calculate the same quantity $\Delta\ell$ with Geant4 methods. For each event, the muon track is selected and, step by step, we use a method that returns the step length $\delta\ell_i$. Then, it is sufficient to sum up all the $\delta\ell_i$ corresponding to steps within the scintillator.

Results

The results obtained with the two different methods are shown in Figure 3.3. Both of the histograms are consistent with the detector geometry and with the angular distribution of muons. The most probable value matches the width of the scintillator (1 cm). Moreover, both of the distributions decrease rapidly for high values of $\Delta\ell$, while they are substantially null between zero and 1 cm.

It is worth noting that the mean value obtained with Geant4 is slightly greater. This might be due to the fact that Geant4 takes into account the multiple scattering.

To verify that the difference between the two histograms is indeed due to the interactions with the material, a test has been performed. This test consists in turning off the multiple scattering. By doing so, it turned out that the overlapping between the two histograms visibly increased. Then, all the other physical processes were turned off, thereby achieving a perfect overlapping as shown in Figure 3.4.

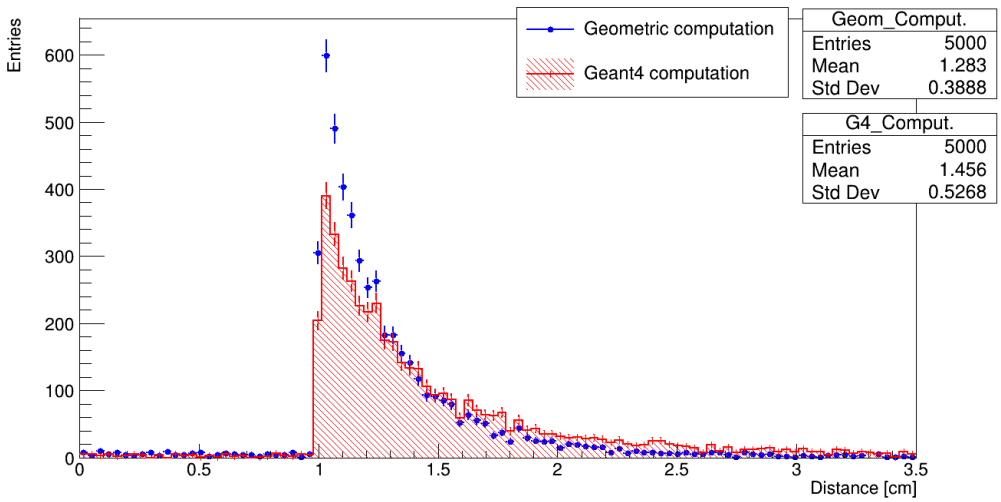

Figure 3.3. Distributions of the distance traveled by muons in the scintillator.

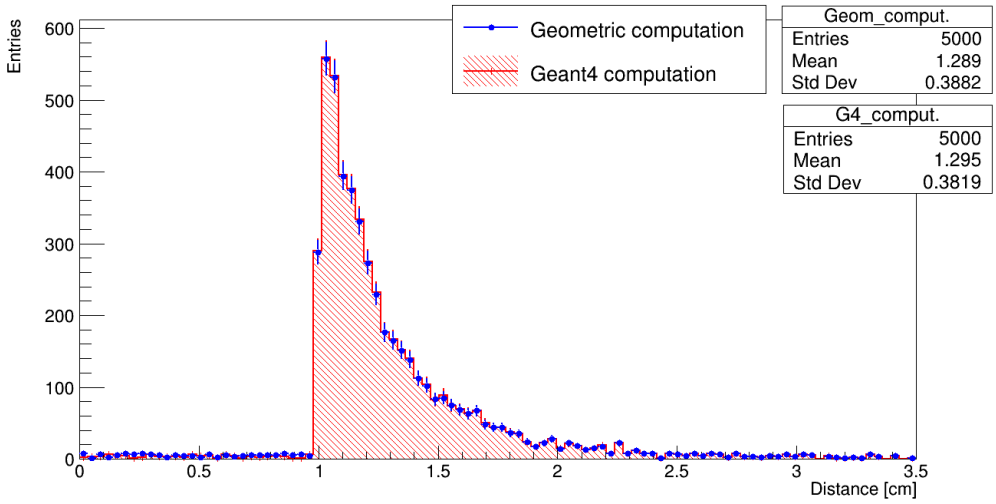

Figure 3.4. Distributions of the distance traveled by muons in the scintillator, when there are no physical processes active.

3.5 Energy loss

It is well known that a charged particle passing through matter loses energy, while being deflected. We have already mentioned the deflection effects in the previous section. The energy loss, instead, is mainly due to inelastic collisions with atomic or molecular electrons of the material. These collisions are stochastic in nature, but since the number of collisions is macroscopically elevated, it is possible to define the average energy loss per unit length $\langle dE/dx \rangle$. This quantity depends on the specific material, as well as on the particle type and its energy. A useful parametrization of this quantity is given by the Bethe-Block formula [2]:

$$-\left\langle \frac{dE}{dx} \right\rangle = 4\pi N_e r_e^2 m_e c^2 \frac{z^2}{\beta^2} \left(\ln \frac{2m_e c^2 \beta^2 \gamma^2}{I} - \beta^2 - \frac{\delta(\gamma)}{2} \right) \tag{3.4}$$

where:

- m_e and r_e are, respectively, the mass and the classical radius of the electron;
- I is the ionization potential of the atomic structure of the target;
- β is the ratio between the particle velocity and the light speed;
- γ is the Lorentz factor, namely $\gamma = \dfrac{1}{\sqrt{1-\beta^2}}$;
- $\delta(\gamma)$ is a density correction that, for high energy particles, reduces the logarithm growth.

A graph of the $\langle dE/dx \rangle$ for muons on copper is shown in Figure 3.5.

To calculate the total energy loss, we can either perform a simplified computation, by integrating the $\langle dE/dx \rangle$ given by the Bethe-Block formula, or use Geant4 classes and methods.

Simplified computation

The use of only Bethe-Block formula implies two approximations:

The first approximation is due to the fact that the energy loss expressed by (3.4) represents a mean value. In fact, two models describe the fluctuations of dE/dx: in case of thick absorbers, a significant number of collisions occur, hence the *Central Limit Theorem* holds, and dE/dx fluctuates as a Gaussian distribution; for thin absorbers, instead, dE/dx is distributed as a non-symmetrical function (a Landau function) whose mean value is greater than its most probable value.

The second approximation consists in assuming the overall energy loss of a particle much smaller than its initial energy so as to consider $\langle dE/dx \rangle$ constant

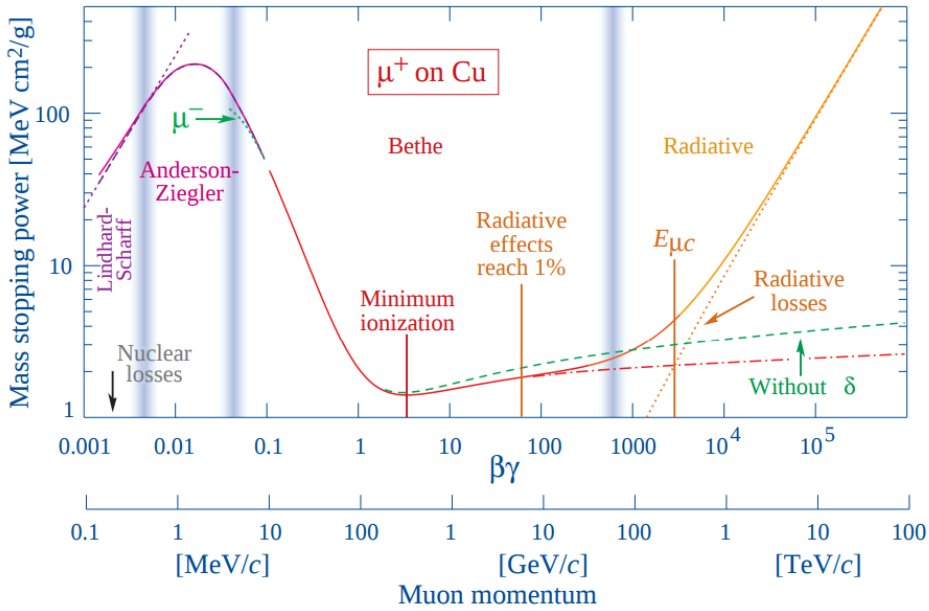

Figure 3.5. Mass stopping power as function of $\beta\gamma$ (or momentum) of muons on copper [5].

and hence simplify the integration. This approximation, besides being verified ex-post, is reasonable for muons with $E_0 = 1$ GeV that pass through ~ 1 cm of scintillation material.

Geant4 computation

By analogy with the earlier computation of $\Delta\ell$, the energy losses δE_i for each step were calculated by Geant4 and summed up, thus achieving the total energy loss ΔE. It is important to remember that Geant4 in this case reproduces all the allowable processes (in particular, the energy loss described by the Bethe-Block formula as well).

As a test, the quantity $\Delta E/\Delta\ell$ has been computed, and its value as a function of the particle energy is shown in Figure 3.6. In order to compare this result with the $\langle dE/dx \rangle$ shown in Figure 3.5, the scintillator material has been momentarily changed into copper. Moreover, all the physical processes, apart from the ionization, have been turned off.

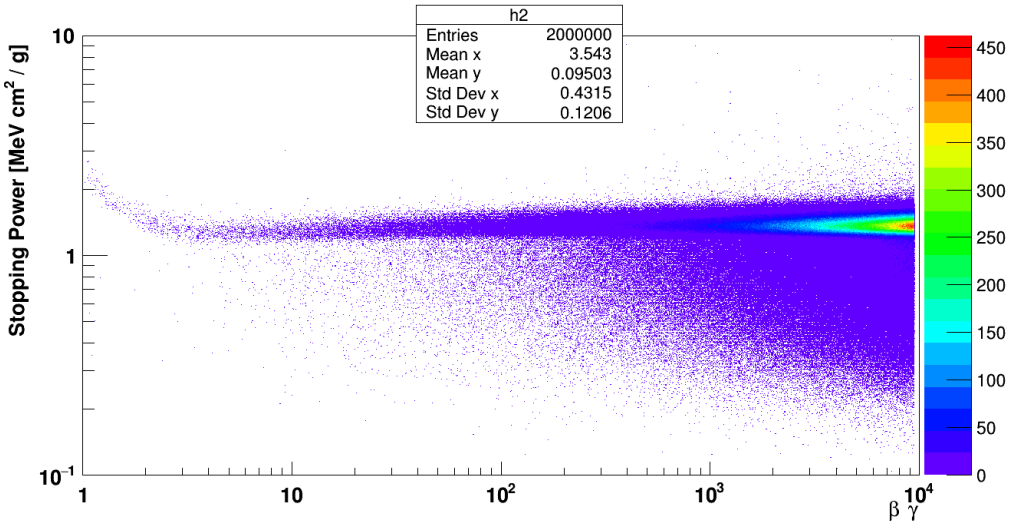

Figure 3.6. Plot of the $\Delta E/\Delta\ell$ as a function of $\beta\,\gamma$

Within the statistical fluctuations we notice a similar trend to that in Figure 3.5, especially at minimum ionization .

Results

The total energy loss ΔE for a 1cm-thick copper plate has been computed. The two histograms so obtained are shown in Figure 3.7. It is worth noting that the application of only the Bethe-Block formula gives a mean value greater with respect to the other method. This difference occurs because the mean value of dE/dx is greater than the most probable value for thin absorbers.

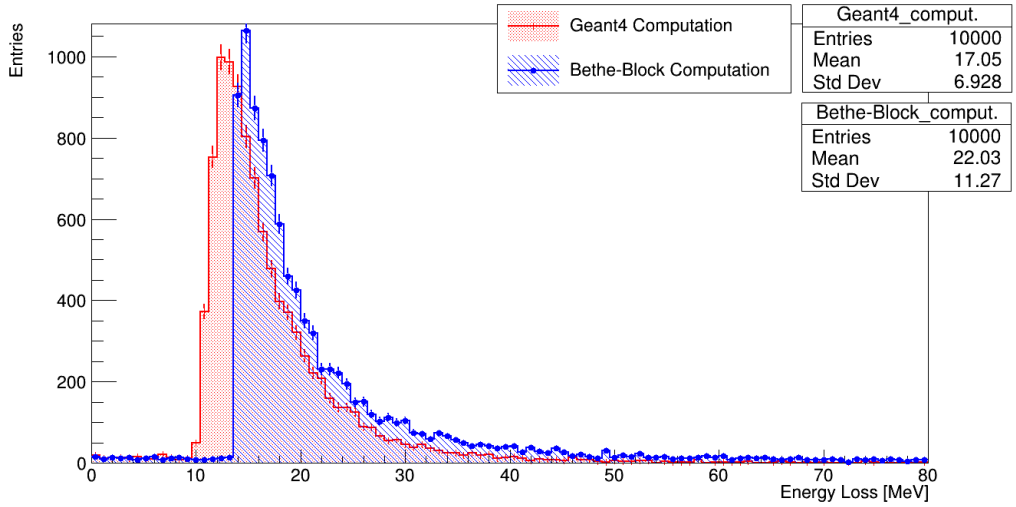

Figure 3.7. Distributions of ΔE for 1 GeV muons on copper.

3.6 Scintillation

As previously mentioned, any material is characterized by its *light yield* ε, i.e., the average number of photons emitted as a function of the energy loss. If we fix ε, then the number of photons emitted n_{γ_i}, to a first approximation, follows a Poisson distribution with mean value $\langle n_{\gamma_i} \rangle = \varepsilon \, \Delta E$. However, ionization processes are not completely unrelated among them, since they depend on the electronic shells [2]. Thus, a simple Poisson distribution cannot be used. However, we can make a correction on the standard deviation:

$$\sigma = R \, \sigma_{pois} = R \sqrt{\langle n_{\gamma_i} \rangle} \tag{3.5}$$

where, in Geant4, R denotes the parameter which modifies the energy resolution of the scintillator. For instance, materials with a small Fano factor have a good resolution.

In Geant4, it is possible to set both ε and R for a given material, and, in this case, we have set the following values: $\varepsilon = 5000$ MeV^{-1} and $R = 10$ (such a large value of R will be useful for seeing some effects later).

It is important to note that in Geant4 the light yield is linearly dependent on the energy loss ΔE, but this is only an approximation as the efficiency of scintillators, in reality, also depends on the particle type and its energy.

Counting of emitted photons

On the basis of what we have discussed so far, and having defined the values of ε and R as above, we can compute the number of photons emitted when a 1 GeV muon passes through the scintillator perpendicularly. Figure 3.8 and Figure 3.9 represent respectively the distribution of the energy loss ΔE and the distribution of the number of photons emitted. The two histograms relate to the same run (1000 muons hitting vertically).

Since Δx is now the same for each event, the distribution of ΔE is a Landau distribution – specific of thin absorbers. The distribution of the number of photons emitted has a similar shape, but with a multiplicative factor of ~ 5000 MeV^{-1}, namely the value of ε. Moreover, this second distribution results widened by the factor $R = 10$ (previously set).

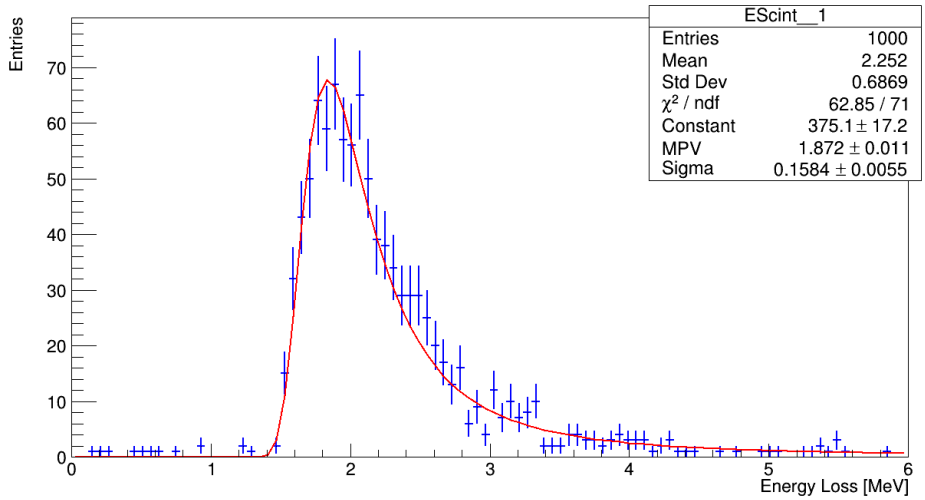

Figure 3.8. Energy loss distribution for 1 GeV muons impacting perpendicularly. A Landau function has been fitted to the histogram.

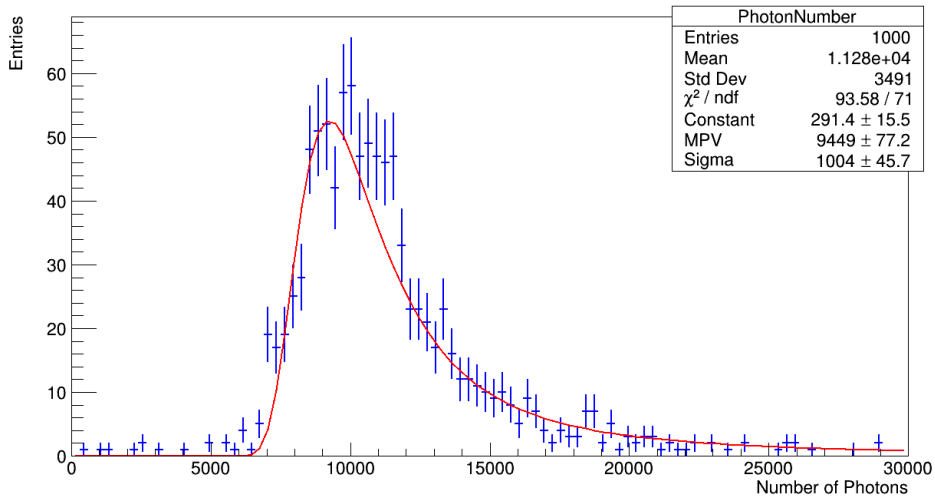

Figure 3.9. Distribution of the number of photons emitted for 1 GeV muons, impacting perpendicularly. A Landau function has been fitted to the histogram.

Energy spectrum of photons

Scintillators, like any material, have an emission spectrum that can be considered continuum because of the rotational energy levels of the material's molecules. In the specific case, the spectrum has been set as in Figure 3.10. We made this choice by considering the maximum brightness of the plastic scintillator UPS89 (470 nm) [3].

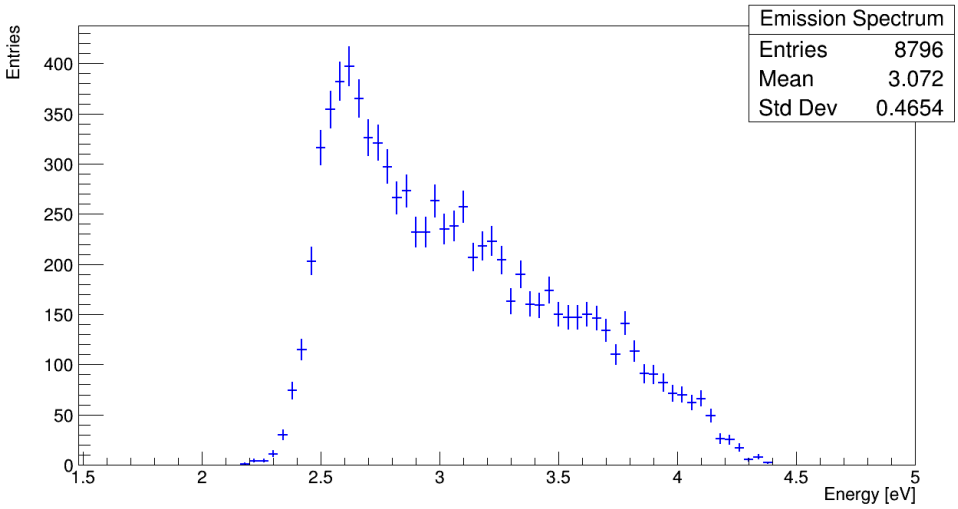

Figure 3.10. Emission spectrum of the scintillator.

Time evolution of photon emission

Two components of the photon emission can be distinguished: a fast and slow one, both with an exponential time evolution. However, in the simulation, the slow component has not been reproduced since scintillation detectors exploit the fast emission only.

We have set the characteristic time of the fast component based on the UPS89 scintillator features [3], namely $\tau_f = 1$ ns. In the next section, the arrival time of photons at the photocathodes will be studied, and further observations shall be made.

3.7 Light signal propagation

Once the photons are emitted, they propagate through the scintillator undergoing two main processes: internal reflections and reabsorption. Hence, photons that are not absorbed reach one of the two photocathodes.

The internal reflections are enhanced by the reflecting material that covers the scintillator. In the simulation, reflections are implemented by setting the reflectivity r of the surface of the scintillator. To have the maximum reflection number r has been designated as equal to 1, though this is an ideal situation.

The reabsorption, instead, has been implemented by defining the absorption length λ, that is, the free mean path of photons ($\lambda = 360$ cm for the UPS89 scintillator). It is worth noting that both r and λ, in reality, are properties depending on the photon energy, however, to simplify the simulation we fixed these two parameters.

To verify the correct working of this part of the simulation, we have performed two tests: one on the number of photons reabsorbed or collected at the PMT; one on the arrival time of photons at the photocathodes.

For a given event, the number of photons generated ($n_{\gamma_{gen}}$), reabsorbed ($n_{\gamma_{abs}}$) and collected at the photocathodes ($n_{\gamma_{PMT_{1,2}}}$) must fulfill:

$$n_{\gamma_{gen}} = n_{\gamma_{abs}} + n_{\gamma_{PMT_1}} + n_{\gamma_{PMT_2}} \tag{3.6}$$

Moreover, photons are emitted isotropically, hence, for a muon passing along the z axis, the following must be true:

$$\left\langle n_{\gamma_{PMT_1}} \right\rangle = \left\langle n_{\gamma_{PMT_2}} \right\rangle \tag{3.7}$$

The first test concerns 2500 muons passing along the z axis. In this case, it has been verified that the histograms of $n_{\gamma_{gen}}$ (Figure 3.12a) , $n_{\gamma_{abs}}$ (Figure 3.12b) and $n_{\gamma_{PMT_{1,2}}}$ (Figure 3.11) satisfy the 3.7 and the 3.6 (on average). It is worth noting that all four distributions are Gaussian-like with variance compatible with the mean value. Thus, we are dealing with Poisson distributions in the Gaussian limit. The fact that the distribution of $n_{\gamma_{gen}}$ (Figure 3.12a) is slightly wider is due to the R factor previously discussed.

It is important to note that the histogram of $n_{\gamma_{gen}}$ in Figure 3.9 in the previous section differs from the histogram in Figure 3.12a because, in the latter, the energy loss of muons has been kept fixed ($\Delta E = 0.5$ MeV). Thus, there are no Landau fluctuations. Besides, to reduce the computational time, the light yield has been reduced to 1000 MeV^{-1}.

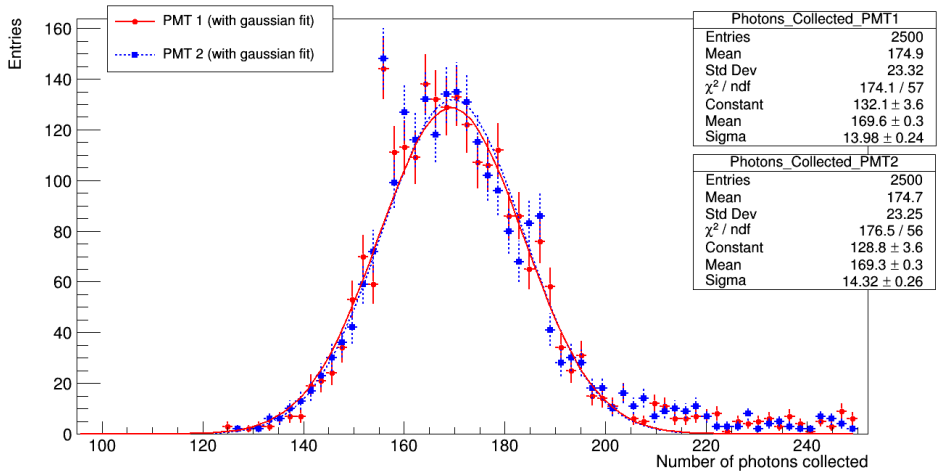

Figure 3.11. Distributions of the number of photons collected at the two photocathodes (PMT1 e PMT2). A Gaussian function has been fitted to both distributions.

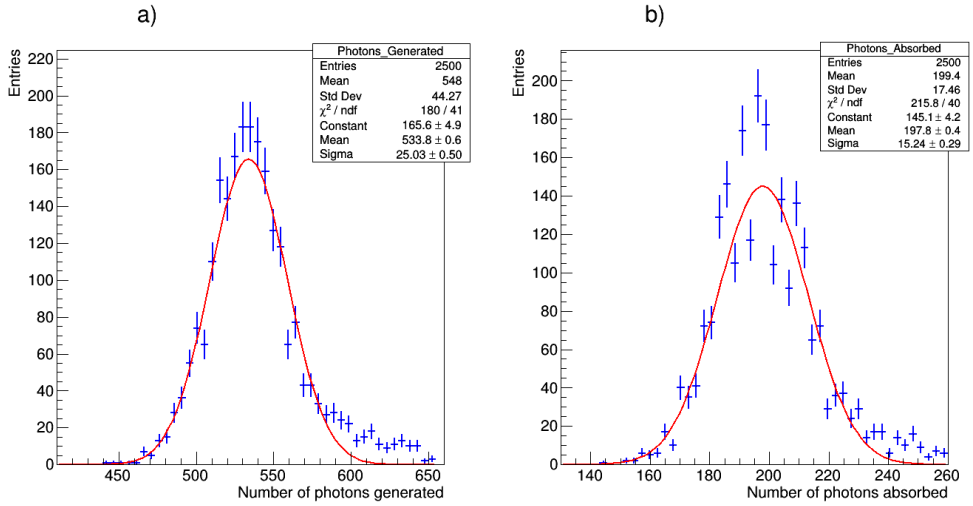

Figure 3.12. Distribution, with Gaussian fit, of the number of photons emitted (a); and distribution, with Gaussian fit, of the number of photons reabsorbed (b).

The second test in this part of the simulation features studying light signals as a function of time.

For a given event, we can produce a distribution that represents the number of photons arriving at a given time at a photocathode. Such a distribution, hence, represents the light intensity against time. To obtain this distribution we have used the methods of Geant4. Furthermore, we emphasize that the temporal zero has not been fixed at the time emission of a photon, but has been chosen to be at the beginning of the whole event, i.e., the temporal instant whene the muon hits the scintillator. This choice is reasonable since the aim of this computation is to reproduce a signal similar to those that are measured at the anode of the real PMT in the laboratory.

It is worthwhile to study the shape of these signals as a function of the distance d between the point of impact of the muon (impacting vertically) and a given photocathode. For this purpose, in Figure 3.13 the results are given for three values of d (1 cm, 21 cm and 121 cm).

From the graphs, it is evident that the greater the distance between the point of impact of the muon and the PMT, the more the signal is delayed. Furthermore, the signal goes to zero more rapidly when it is generated near the photocathode. Indeed, this is the behavior we expect. We also note that for $d = 1$ cm the characteristic time is $\tau_1 \simeq 1.1$ ns, and for $d = 21$ cm it is $\tau_2 \simeq 2.9$ ns. Hence

$$\tau_2 > \tau_1 > \tau_0 = 1 \text{ ns} \tag{3.8}$$

where τ_0 is the characteristic time of the emission of photons in the scintillator, previously set as 1 ns. The fact that the signals go less rapidly to zero than e^{-t/τ_0} (i.e. that their duration increases with d) is probably due to the internal reflections.

Now, let $\bar{t}$ denote the arrival time of the signal, that is, the instant when the signal starts rising. Then, we can estimate the speed of the signal through the scintillator. When d is 21 cm, $\bar{t} \simeq 1.0$ ns; when d is 121 cm, $\bar{t} \simeq 6.4$ ns. Hence, by simple calculations $v \simeq 18.5$ cm/ns $\simeq 0.62c$. This result seems to be consistent in magnitude with the experimental value $v_{exp} \simeq 0.43c$ measured in the Nuclear and Subnuclear Physics Laboratory.

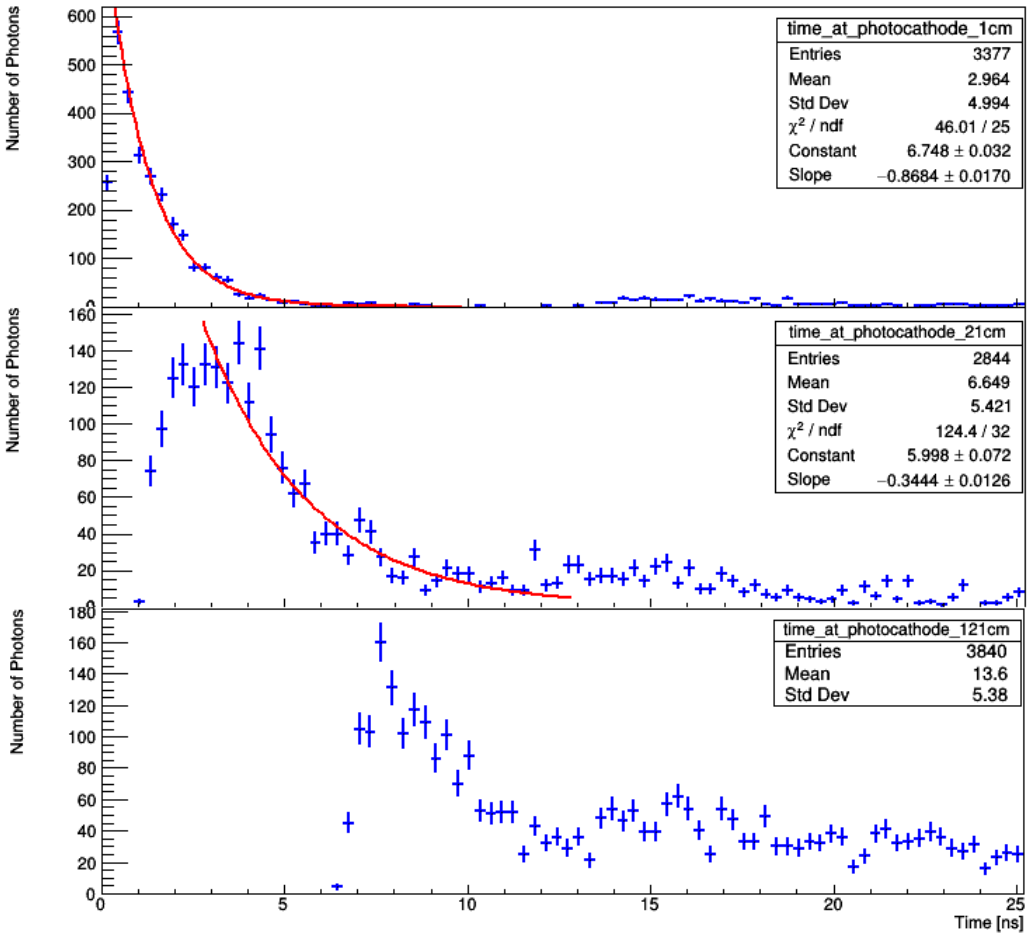

Figure 3.13. From the top downwards, the number of photons at the photocathode against time for a muon impacting 1 cm, 21 cm and 121 cm from the photocathode. An exponential function has been fitted to the tail of the first two distributions.

3.8 Photomultiplier

The implementation of the PMT has been divided into two phases. The first one simulates the photoelectric effect that occurs on the photocathode; the second one reproduces the electro-multiplication process that takes place on the dynodes. As already mentioned, for this part we have used simple algorithms, outside Geant4. These algorithms use the data elaborated so far (arrival time, energy and number of photons at the photocathode).

The characteristics of our PMTs are those of the PMTs Photonis XP2262 used in the laboratory, namely, 12 dynodes, a total gain $G = 5 \cdot 10^7$ and a spectral range between 290 nm and 650 nm.

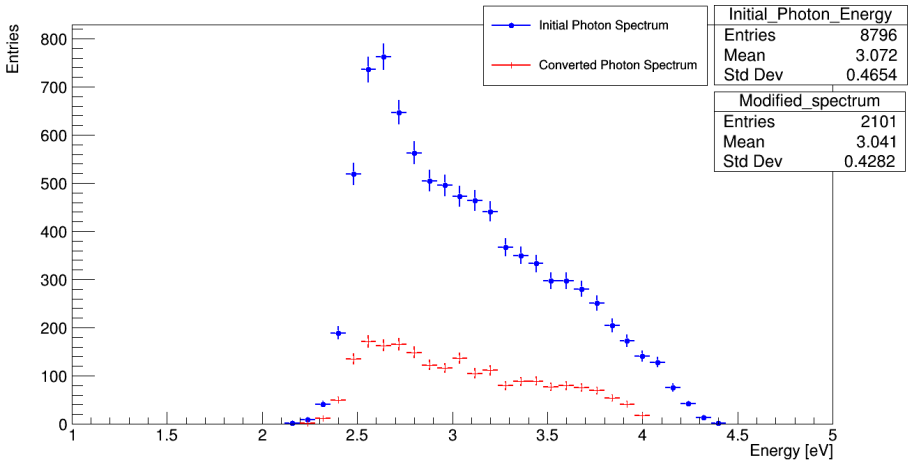

Figure 3.14. Initial spectrum of photons at the photocathode, and spectrum of photons that convert at the photocathode.

Photocathode

When a photon impacts on the photocathode, it can cause the emission of electrons from the photocathode material (i.e., photoelectric effect). The probability of having the photoelectric effect is called *quantum efficiency* (ε_q), and in general, for a photocathode, it barely reaches the 30%. The quantum efficiency depends on the photocathode material, as well as on the photon energy. The dependence on the energy defines the spectral response of the photocathode.

In the specific case, we have set a flat spectrum with $\varepsilon_q = 0.25$ between 2 eV and 4 eV. Therefore, when a photon with the proper energy hits the photocathode, its conversion will be determined by a Bernoulli variable with a 0.25 probability. Besides, since the value of ε_q is constant, the overall number of photons converted is a Poisson variable with a mean value of $0.25 \cdot n_{\gamma_i}$.

Figure 3.14 shows both the initial spectrum of the photons at the photocathode and the spectrum of the photons that convert at the photocathode. It is to be noted that the initial spectrum is essentially the same as the emission spectrum shown precedently in Figure 3.10.

It is worthwhile to stress that the spectrum of photons that convert does not represent the energy spectrum of photoelectrons produced. In fact, once generated, photoelectrons are accelerated by a very strong electric field ($\sim 10^3$ V/cm) that drives them onto the first dynode. Hence, any difference in the initial energy among photoelectrons is negligible with respect to the energy gained (∼keV) after being generated.

Although the simulation of the photoelectric effect has been performed with several simplifications, it remains clear that coupling the emission spectrum of the scintillator with the spectral response of the photocathode is extremely important.

Electro-multiplication

The gain G of a PMT is the average number of secondary electrons generated from a photoelectron. The actual number of secondary electrons fluctuates since the electro-multiplication is stochastic in nature. It is reasonable to assume those fluctuations to be Poissonian, yet, we will treat them as Gaussian, the order of magnitude of G being elevated. Hence, a way to simulate the electro-multiplication is to sample a value of secondary electrons (n_{sec}) from a Gaussian distribution with mean value and variance G.

By sampling n_{sec} for each photoelectron, we will obtain the total number of secondary electrons that reaches the anode. Thus, the overall number of secondary electrons will be the sum of as many Gaussian distributions as the photoelectrons. Figure 3.15a shows the number of secondary electrons for 10000 events. The distribution is Gaussian, indeed, it is well known that the sum of two or more independent Gaussian variables is still Gaussian distributed.

Another way to implement this part of the simulation involves the use of the above computation for every single dynode. In fact, the total gain G can be expressed in terms of the gain g_i of each dynode which is directly proportional to the voltage V_i applied to it. The proportionality constant k_i depends on both the geometry and the material of the dynode. Thus, with n dynodes, the total gain

can be written as:

$$G = \prod_{i=1}^{n} g_i = \prod_{i=1}^{n} k_i V_i \tag{3.9}$$

If we assume all the dynodes to be identical to each other ($k_i = k_j$) and the voltage equally divided by a proper voltage divider ($V_i = V_j$), the (3.9) reads:

$$G \simeq g^n \tag{3.10}$$

By reversing the (3.10), in this specific case ($n = 12$ and $G = 5 \cdot 10^7$), we obtain, on average, 4 secondary electrons generated from each primary electron hitting a given dynode. Hence, the overall number of secondary electrons n_{sec}, generated from a photoelectron, is the product of 12 Poisson variables with a mean value of 4. Furthermore, as for the previous method, all the secondary electrons need to be summed up, so as to obtain the total number of electrons at the anode. If the number of photoelectrons is reasonably large (8000 in this case), according to the *Central Limit Theorem* the overall number of electrons will be Gaussian distributed, as is evident from the Figure 3.15b. For the above observations, the mean values of the two distributions a) and b) are the same, while their standard deviations differ. In particular, the method that implements the electro-multiplication dynode by dynode (b) has a standard deviation extremely greater than the one of the distribution achieved with the other method (a).

Once the electro-multiplication has been implemented, it is possible to obtain the current signal at the anode of a PMT by applying the above fluctuations to the result of section 3.7. To reduce the computational time, the total gain has been decreased (now, $G = 10^5$).
As anticipated, we have disregarded any delay (and its fluctuations) due to the photoelectric effect and the electro-multiplication. Thus, for a given photoelectron produced at the time $\bar{t}$, the secondary electrons are assumed to arrive at the anode all at the same $\bar{t}$. The simulation of the electro-multiplication relates to an event whose light signal is shown in the previous Figure 3.13 (central). The corresponding current signal is shown in Figure 3.16a together with a real signal generated by a scintillator in the laboratory (Figure 3.16b). For a better comparison, the origin of the temporal axis has been translated so as to match the origin of the temporal axis of the simulation.

Of course, the real signal is purely illustrative, and it is only possible to perform a qualitative comparison between the two graphs a) and b) in Figure 3.16: both signals are characterized by a rapid initial rise; the duration of the simulated signal is slightly shorter, but, as we have already discussed, this feature might depend on many factors, including the relative position between a PMT and the impacting point of the muon.

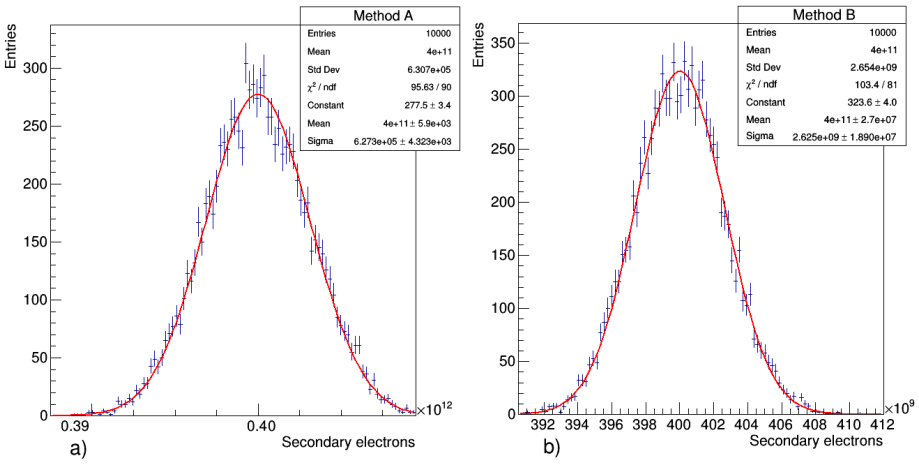

Figure 3.15. Distributions of the number of secondary electrons generated from 8000 photoelectrons, when considering the total gain (a), or simulating the electro-multiplication on each dynode (b). A Gaussian function has been fitted to both of the histograms.

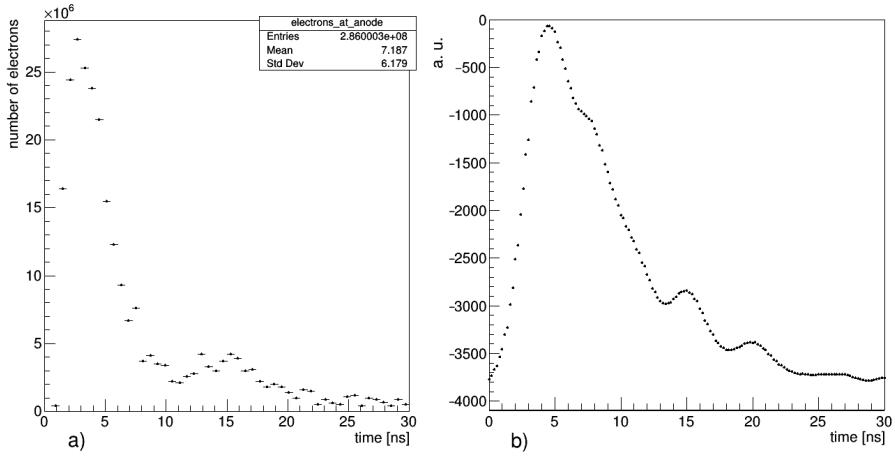

Figure 3.16. a) Arrival time of the electrons at the anode. b) Signal in arbitrary units generated by a scintillator in the laboratory.

To conclude this section, it is worthwhile to note that the implementation of the electro-multiplication has been performed with a significant degree of simplification since we have not taken the spectral response of dynodes into consideration. In fact, each dynode should be treated in the same manner as we have done with the photocathode. However, fluctuations due to the electro-multiplication are small since the current signal in Figure 3.16a and the light signal in Figure 3.13 (central) only differ in normalization factor (the ratio between the two normalization factors is $G = 10^5$). The overall shape of the signal remains, instead, unchanged as proof that the fluctuations discussed above are negligible.

Chapter 4

Conclusion

This work has produced good results which are consistent with the theory and the experimental data. Furthermore, this work has made it possible to apply a model for the energy loss for charged particles passing through matter (Bethe-Block formula), as well as to verify the symmetries of the detector, and study the shape of light (and current) signals as a function of the point of impact of muons. Such signals – qualitatively similar to those produced in the laboratory – have led us to estimate the speed of propagation of the light signal in the scintillator. The value obtained ($v_{sim} \simeq 0.62c$) is comparable with the order of magnitude of the experimental value ($v_{exp} \simeq 0.43c$).

Despite several simplifications, the simulation has allowed us to better understand the different processes involved in the working of scintillation detectors, and distinguish the parameters that define their performances. Ultimately, we became aware of the fundamental importance of simulation methods in particle physics.

Appendix A

Simulation code

The source of the simulation program is briefly described here.

As shown in Figure A.1, in the main directory, there are the '*main*' program (`AnaEx01.cc`) and two subdirectories, `include` and `src`, which contain respectively *header files* (`*.hh`) and *source code files* (`*.cc`) of the classes used in the simulation.

The example AnaEx01 of Geant4 was taken as a starting point to implement the simulation. This example is available in the following Geant4 directory: `examples/extended/analysis`. In particular, we used the same modes of creation, filling and management of the histograms as in the example. We left the structure of the working directory shown in Figure A.1 as it was in the example. However, all the classes were extensively enriched and modified.

The source can be found at the following link:

`https://github.com/pietro14/G4-Simulation.git`

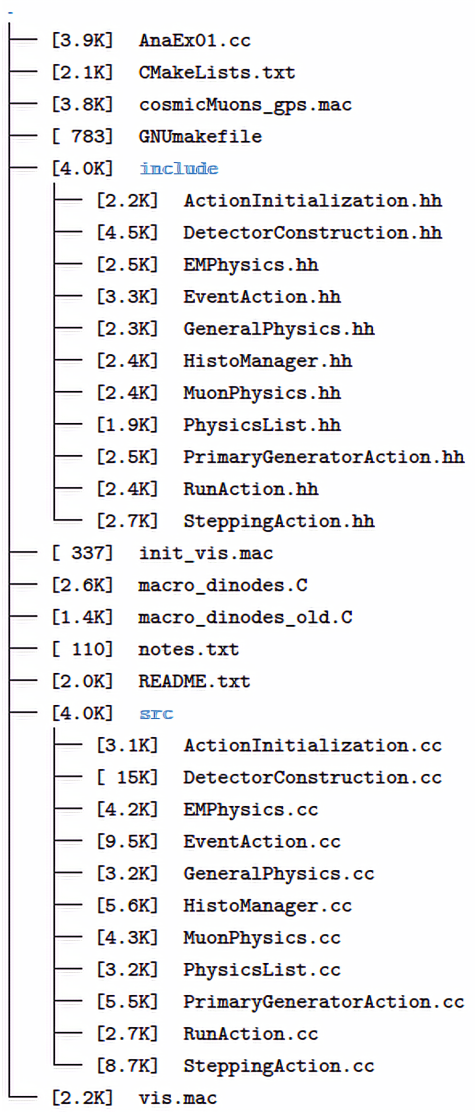

Figure A.1. Working directory containing the simulation code. The size of each file is in squared brackets.

Bibliography

[1] Geant4 Collaboration, "Book For Application Developers, Release 10.4", 2007, `https://www.ge.infn.it/geant4/training/ptb_ 2009/literature` (link valid on the 15th Oct. 2018)

[2] W. R. Leo, *Techniques for nuclear and particle physics experiments*. Springer-Verlag, 1994.

[3] R. C. Fernow, *Introduction to experimental particle physics*. Cambridge Univ. Press, 2001.

[4] F. Ceradini, "Appunti del corso di istituzioni di fisica nucleare e subnucleare," Gen 2003.

[5] H. Bichsel, D. Groom, and S. Klein, "33. passage of particles through matter - particle data group," Aug 2015.